Structural analyses of RuO_2-TiO_2/Ti and IrO_2-RuO_2-TiO_2/Ti anodes

used in industrial chlor-alkali membrane processes

Yoshio Takasu* and Wataru Sugimoto

Department of Materials and Chemical Engineering, Faculty of Textile Science and

Technology, Shinshu University, 3-15-1 Tokida, Ueda, Nagano 386-8567, Japan

Yoshinori Nishiki, Syuji Nakamatsu

Permelec Electrode Ltd, 2023-15 Endo, Fujisawa, Kanagawa 252-0816, Japan

Abstract

The morphology and composition of RuO_2-TiO_2/Ti and IrO_2-RuO_2-TiO_2/Ti anodes, which have been used for the production of chlorine for more than 10 years, were analyzed by various methods; such as high-resolution scanning electron microscopy (HR-SEM), high-resolution Auger electron spectroscopy (HR-AES), electron probe X-ray emission microanalysis (EPMA) and X-ray diffraction analysis (XRD). Drastic changes in the surface morphology, including partial exfoliation of a small amount of the oxide layer and a reduction in the content of ruthenium species through dissolution, were observed for the RuO_2-TiO_2/Ti anode. For the IrO_2-RuO_2-TiO_2/Ti anode, on the other hand, there were moderate changes in the surface morphology and moderate dissolution of iridium and ruthenium species.

Keywords: Iridium oxide, Ruthenium oxide, Titanium oxide, Anode, Chlorine evolution

* Corresponding author

E-mail address: ytakasu@shinshu-u.ac.jp (Y. Takasu)

1. Introduction

The electrolysis of brine, a concentrated aqueous solution of sodium chloride, used for the production of chlorine, sodium hydroxide and hydrogen, is an important industrial electrochemical process. Since the anode of the electrolysis process is exposed to a highly oxidative environment in a weak acid solution during the electrolysis, anti-corrosive oxide-coated dimensionally stable anodes, called DSA[®] or DSE[®], have usually been used worldwide. After the development of the DSA[®] [1], both fundamental and applied researches have been carried out as reviewed by Trasatti [2-4]. For instance, industrial applications for chlor-alkali processes [5-11]; the form of Ti substrates (e.g., nets, meshes, expanded metals) of the DSA[®]s used in industry [8-11]; the optimum chemical composition such as RuO_2 (30%)-TiO_2(70%)/Ti [12-14]; recommended preparation temperature (e.g., 400~500°C for RuO_2-TiO_2/Ti) [13, 15]; surface area (roughness factor) of oxide electrodes such as IrO_2-RuO_2/Ti electrodes [16-18]; observation of the mud-cracks by scanning electron microscopy [19, 20]; effect of the preparation conditions on the formation of solid-solution (e.g., RuO_2-TiO_2/Ti) [21, 22]; observation of the enrichment of the surface with particular species such as TiO_2 or IrO_2 by electron spectroscopy [23-27]; effect of IrO_2 to RuO_2 or RuO_2-TiO_2 on the durability of the DSA[®]s [16-18, 27-31]; preparation of oxide powders such as RuO_2-TiO_2, IrO_2-RuO_2-TiO_2 and IrO_2-RuO_2 to clarify the stable crystal structure of the binary and ternary oxides [32-34]; single-crystal oxide electrodes, RuO_2 for example, to investigate the real catalytic property of oxide electrodes [35]; oxygen evolution activity of IrO_2 for the electro-plating [3, 36-41]. The morphology, crystal structure, and composition of DSA[®]-type electrodes have been characterized by many research scientists; however, the

precise durability of the anodes used in industry has not yet been determined. Typical DSA$^®$s used in chlor-alkali processes are RuO_2-TiO_2/Ti and IrO_2-RuO_2-TiO_2/Ti, in which both ruthenium and iridium species act as catalysts for the chlorine evolution and iridium enhances the durability of the RuO_2-TiO_2 oxide layer.

In the present investigation, the oxide layers of RuO_2-TiO_2/Ti and IrO_2-RuO_2-TiO_2/Ti anodes, which were applied in two different electrolytic cells, were characterized and compared with those of pristine specimens. The information on these typical DSA$^®$s must contribute to not only the improvement of DSA$^®$s but also to the design of new oxide-coated electrocatalysts.

2. Experimental

2.1 Test electrodes

Optical micrographs of the RuO_2-TiO_2/Ti and the IrO_2-RuO_2-TiO_2/Ti anodes analyzed in this investigation are shown in Fig. 1. Both electrodes have a characteristic low overpotential for chlorine evolution in chlor-alkali membrane cells. The RuO_2-TiO_2/Ti electrode has been used for 12 years at average current density of 4 kA m^{-2}. The IrO_2-RuO_2-TiO_2/Ti electrode with an initial molar ratio of Ir:Ru = 1:1 has been used for 15 years of the chlorine evolution in industry at average current density of 3 kA m^{-2}. For both electrodes, the parts that were not exposed to the electrolyte were regarded as pristine specimens in this study. In this investigation, the surface of the anodes facing the membrane during the electrolysis was analyzed.

2.2 Characterization methods of the electrodes

The morphology and the composition of the electrode specimens were analyzed by high-resolution scanning electron microscopy (HR-SEM; Hitachi S-5000), high-resolution

Auger electron spectroscopy (HR-AES; Physical Electronics Inc., Model 680. The diameter of the incident electron beam was 35 nm. Evaluation of the elements; Ti; LMM Auger peaks, Ir; MNN Auger peaks, Ru; MNN and LMM Auger peaks), and electron probe X-ray emission microanalysis (EPMA, JEOL, JXA-8600MX). The crystal structure of the oxide layer of the electrodes was characterized by X-ray diffraction analysis (XRD, Rigaku RINT-2550, CuK_α).

3. Results and Discussion

3.1 The RuO_2-TiO_2/Ti electrode

3.1.1 Morphology of the oxide layer

Figure 2 shows HR-SEM images at various magnifications of the surface of the pristine RuO_2-TiO_2/Ti electrode. The following morphological characteristics were observed; (1) an apparently flat part, (2) crystallites with 50 nm~2 μm in diameter scattered on the flat part, and (3) mud cracks. Even the apparently flat surface observed at lower magnifications was composed of small connected particles that formed narrow apertures (Fig. 2-(d)).

After used for 12 years, the anode showed drastic changes in the surface morphology (Fig. 3): partial exfoliation of the surface layer occurred at various places, crystallites with 50 nm~2 μm in diameter on the flat part disappeared, and small crystallites with 20~60 nm in diameter were exposed on the exfoliated part. Figure 4 is cross-sectional SEM images of the pristine and the used anodes. A stacked oxide with 20 layers was clearly observed on both SEM images. The number of the stacked layers corresponds to the coating times. Thus, the layered oxide structure of these anodes was almost maintained even after the 12-year anodic polarization. The black part "G" shown in Fig.4-(a) is a gap formed, as a result of the cross-sectional cutting, between the oxide layer and the Cu layer which was plated onto the RuO_2-TiO_2/Ti electrode to stabilize the oxide layer towards the cross-sectional cutting.

In the case of the used anode, a few voids smaller than 1 μm in diameter are observed (Fig. 4). Although the smaller voids were also observed in the oxide layer of the pristine electrode, the voids observed in the used anode must have been formed through the dissolution of oxide species during electrolysis. Thus, the dissolution of the oxide species must have occurred not only from the surface but also from inner part of the oxide layer.

3.1.2 Composition and structure of the oxide layer

Figure 5 shows the SEM images with the point analysis data determined by the HR-AES for the pristine and the used anodes. The quantitative analysis of the content of ruthenium, titanium and oxygen is difficult due to the heterogeneity in the composition. The elements detected by the spot analysis are presented only for the characteristic parts. In every crystallite on the pristine electrode, Ru, Ti and O were detected, while no appreciable amount of Ru was detected on the flat part. The enrichment of the titanium oxide on the surface of the flat part must be caused, at least partially, not only by the higher reactivity of titanium precursor than that of ruthenium precursor but also by the diffusion of titanium ions from the titanium substrate. On the other hand, Ru was not detected anywhere on the used electrode by the HR-AES. Even though no Ru species existed in the surface layers, the electrode is still active for the chlorine evolution. This suggests that the electrolyte reaches the Ru sites in the inner layer of the porous anode where the electrolysis proceeds. The EPMA analysis of the oxide layer before and after the polarization showed that the 12-years anodic polarization resulted in considerable loss of ruthenium of up to 43% from the RuO_2-TiO_2 layer.

The XRD patterns of the electrode before and after the polarization are shown in Fig. 6. No evident decrease in the intensity of the diffraction peaks from the oxide by the polarization was observed. No shift of the diffraction peaks was observed even after the 12-years polarization.

3.2 The IrO$_2$-RuO$_2$-TiO$_2$/Ti electrodes

3.2.1 Morphology of the oxide layer

Figure 7 shows HR-SEM images of the surface of the pristine IrO$_2$-RuO$_2$-TiO$_2$/Ti electrode at various magnifications. The surface was heterogeneous in morphology and composed of granules with a few micrometers in diameter and needle-like crystallites grown both on the granules and from the aperture of each granule. Even apparently flat granules at lower magnifications were composed of small connected particles, ca. 10~20 nm in diameter, which formed narrow apertures and cracks. The needle-like crystallites, clarified at the higher magnification, were square columnar crystallites (Fig. 7-(c)). The HR-SEM images of the anode used for 15 years showed that a drastic change in the surface morphology occurred as a result of polarization (Fig. 8). In other words, the granules and square columnar crystallites with 10~30 nm in diameter became evident, so did the corrosion of the edges of the square columnar crystallites.

In Fig. 9, a cross-sectional SEM image of the pristine anode is compared with the polarized one. Unlike the case of the RuO$_2$-TiO$_2$/Ti electrode, the layered oxide structure was unclear except for that near the surface of the pristine electrode. Although a few layers near the surface of the pristine electrode were dark-gray, the dark-gray layer increased to about one third of the width of the oxide-coating in the polarized one. Thus, the selective dissolution of the conductive component of the oxide coating proceeded by the 15-years polarization must be responsible for the increase in the width of the dark-gray layer, while the difference in the composition for the two layers, shown as white and dark-gray layers in the SEM image, has not been characterized.

3.2.2 Composition and structure of the oxide layer

Figure 10 shows SEM images with the point analysis data determined by the HR-AES for the pristine and the used IrO$_2$-RuO$_2$-TiO$_2$/Ti anode. In every crystallite on the pristine electrode, Ir, Ru, Ti and O were detected, while no appreciable amounts of Ir and Ru were

detected on the flat part. The enrichment of the titanium oxide on the flat part must be caused, at least partially, not only by the higher reactivity of titanium precursor than those of the other metal precursors but also by the diffusion of titanium ions from the titanium substrate. Differently from the case of the RuO_2-TiO_2/Ti anode, precious elements could be detected anywhere after the polarization on the used electrode, with the exception of some parts analyzed by the HR-AES. The EPMA analysis of the oxide layer before and after polarization showed that the 15-years anodic polarization caused slight losses of iridium (15%) and ruthenium (14%) from the IrO_2-RuO_2-TiO_2 layer.

The XRD patterns of the electrode before and after the polarization are shown in Fig. 11. No evident decrease in the intensity of the diffraction peaks from the oxide was observed. No evident shift of the diffraction peaks was observed even after the 15-years polarization.

4. Summary

The surface morphology, cross-section profile, and composition of the oxide layer of RuO_2-TiO_2/Ti and those of IrO_2-RuO_2-TiO_2/Ti anodes, which have been used for the industrial production of chlorine for 12 and 15 years, respectively, were characterized by various methods. For the RuO_2-TiO_2/Ti anode, considerable dissolution of ruthenium species (43%) and partial exfoliation of the oxide layers were observed. Although the layered oxide structure of the anode was almost maintained, some amount of dissolution of the oxide species from the inner layer was observed, forming voids with smaller than 1 μm in diameter. For the IrO_2-RuO_2-TiO_2/Ti anode, a slight loss of the content of iridium (15%) and ruthenium (14%) was observed. The square columnar crystallites on the surface were also somewhat etched by the lengthy anodic polarization. The cross-sectional SEM image of the anode polarized for 15-years suggested the altered region by the selective dissolution of the conductive component of the oxide coating. The information on the structural analyses for these typical DSA®s used for more than ten years in industries must contribute to not only the

improvement of DSA®s but also to the design of new oxide-coated electrocatalysts.

References

[1] Beer HB (1965) Brit Patent 1 147 442

[2] Trasatti S (2000) Electrochim Acta 45:2337

[3] Trasatti S (2000) Electrochim Acta 36:225

[4] Trasatti S (1999) In: Wiekowski A (ed.), Interfacial Electrochemistry: Theory, Practice, Applications, Marcel Dekker, New York

[5] De Nora O (1970) Chem-Ing-Tech 42:222

[6] Beer HB J Electrochem Soc (1980) 127:301C

[7] Nishiki Y, Nakamatsu S, Aoki K, Tokuda K (1989) J Appl Electrochem 19:90

[8] Horacek J, Puschver S (1971) Chem Eng Prog 67:71

[9] De Nora O (1971) Chem-Ing-Tech 43:182

[10] Nidola A (1981) In: Trasatti S, Lodi G (eds.) Electrodes of Conductive Metallic Oxides, Part B, Elsevier, Amsterdam, p. 627

[11] Koziol KR, Sieberer KH, Rathjen HC, Zenk JB, Wenk EF (1977) Chem-Ing-Tech 49:288

[12] Comninellis Ch, Vercesi GP (1991) J Appl Electrochem 21:136

[13] Hine F, Yasuda M, Yoshida T (1977) J Electrochem Soc 124:500

[14] Veselovskaya IE, Spasskay EK, Sokolov VA, Tkachenko VI, Yakimenko LM (1974) Soviet Electrochem 10:62

[15] Burke LD, Murphy OJ (1979) J Electroanal Chem Interfacial Electrochem 96:19

[16] Yeo RS, Orehotsky J, Visscher W, Srinivasan S (1981) J Electrochem Soc 128:1900

[17] Roginskaya YE, Varlamova TV, Goldstein MD, Belova ID, Galyamov BS, Shifrina RR, Shepelin VA, Fateev VN (1991) Mater Chem Phys 30:101

[18] Savinell RF, Zeller III RL, Adams JA (1990) J Electrochem Soc 137:489

[19] Pizzini S, Buzzanca G, Mari C, Rossi L, Torchio S (1972) Mat Res Bull 7:449

[20] Barral G, Guitton J, Montella C, Vergara F (1977) Surface Technol 6:39

[21] Angelinetta C, Trasatti S, Atanasoska LD, Minevski ZS, Atanasoski RT (1989) Matr Chem Phys 22:231

[22] Gerrard WA, Steele BCH (1978) J Appl Electrochem 8:417

[23] Atanasoska Lj, Atanasoski RT, Trasatti S (1990) Vacuum 40:91

[24] Kondintsev IM, Trasatti S, Rubel M, Wieckowski A, Kaufher N (1992) Langmuir 8:283

[25] de Battisti A, Lodi G, Cappadonia M, Battaglin G, Kötz R (1989) J Electrochem Soc 136:2596

[26] Kameyama K, Tsukada K, Yahikozawa K, Takasu Y (1993) J Electrochem Soc 140:966

[27] Kameyama K, Tsukada K, Yahikozawa K, Takasu Y (1994) J Electrochem Soc 141:643

[28] Faita G, Fiori G (1972) J Appl Electrochem 2:31

[29] Kötz R, Stucki S (1985) J Electrochem Soc 132:103

[30] Kötz R, Stucki S (1986) Electrochim Acta 31:1311

[31] Gorodetskii VV, Neburchilov VA, Pecherskii MM (1994) Russian J Electrochem 30:916

[32] Kameyama K, Shohji S, Onoue S, Nishimura K, Yahikozawa K, Takasu Y (1993) J Electrochem Soc 140:1034

[33] Takasu Y, Onoue S, Kameyama K, Murakami Y, Yahikozawa K (1994) Electrochim Acta 39:1993

[34] Murakami Y, Miwa K, Ueno M, Ito M, Yahikozawa K, Takasu Y (1994) J Electrochem Soc 141:L118

[35] Huang YS, Park HL, Pollak FH (1983) Mater Res Bull 17:1305

[36] Trasatti S (1984) Electrochim Acta 29:1503

[37] Comninellis Ch, Veercesi GP (1991) J Appl Electrochem 21:335

[38] Vercesi GP, Salamin JY, Comninellis Ch (199) Electrochim Acta 36-451

[39] Mousty C, Fóti G, Comninellis Ch, Reid V (1991) Electrochim Acta 45:991

[40] Fierro S, Nagel T, Baltruschat H, Comninellis Ch (2007) Electrochem Commun 9:1969

[41] Ouattara L, Fierro S, Frey O, Koudelka M, Comninellis Ch (2009) J Appl Electrochem 39:1361

Figure captions

Fig. 1   The RuO_2-TiO_2/Ti and IrO_2-RuO_2-TiO_2/Ti anodes

(a) RuO_2-TiO_2/Ti; expanded Ti mesh, (b) IrO_2-RuO_2-TiO_2/Ti; circularly perforated Ti plate.

Fig. 2   HR-SEM images at various magnifications of the pristine RuO_2-TiO_2/Ti anode

Fig. 3   HR-SEM images at various magnifications of the RuO_2-TiO_2/Ti anode used for 12 years.

Fig. 4   Cross-sectional SEM images of the pristine and used RuO_2-TiO_2/Ti anodes

(a); pristine, (b); used for 12 years. The RuO_2-TiO_2/Ti anodes were coated with copper to stabilize the oxide layer towards the cross-sectional cutting. The mark "G" in the left SEM image indicates the gap between the oxide layer and the Cu layer formed by the cross-sectional cutting process.
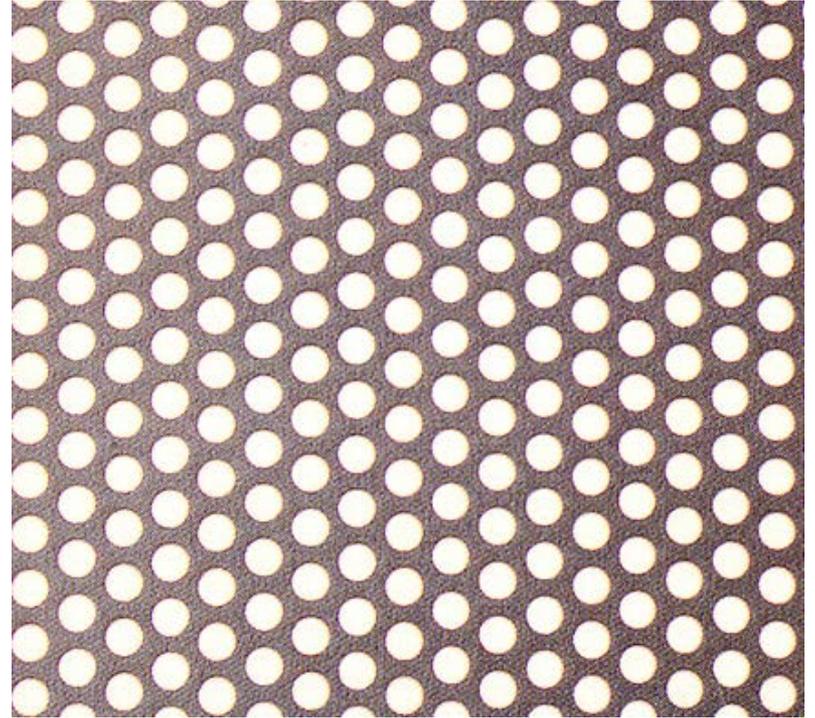
Fig. 5   SEM images with the point analysis data determined by the HR-AES for the pristine and the used RuO_2-TiO_2/Ti anodes.
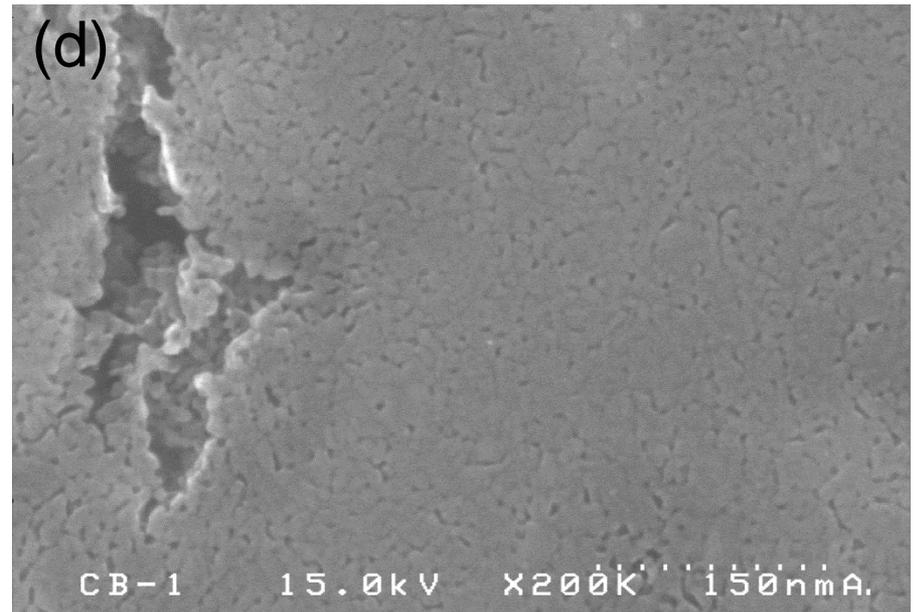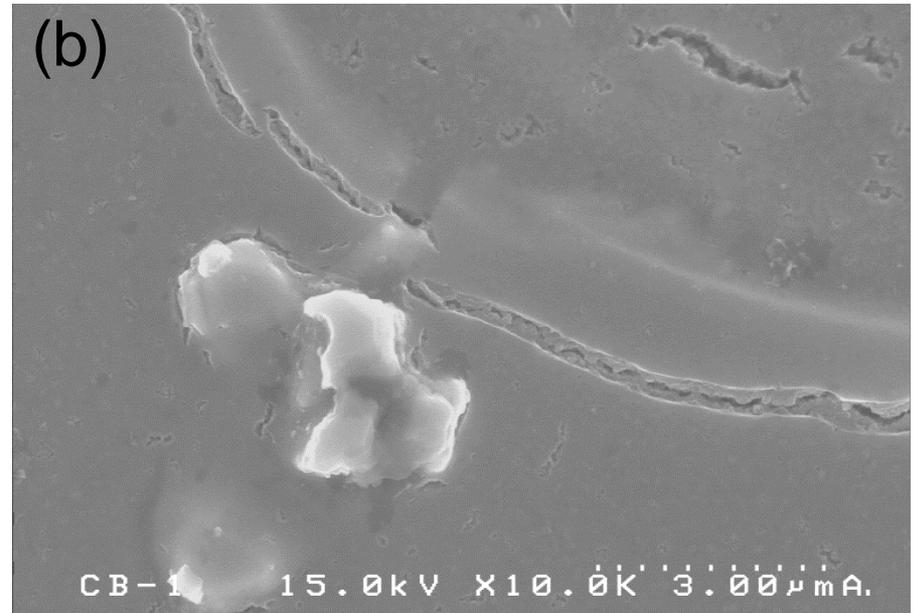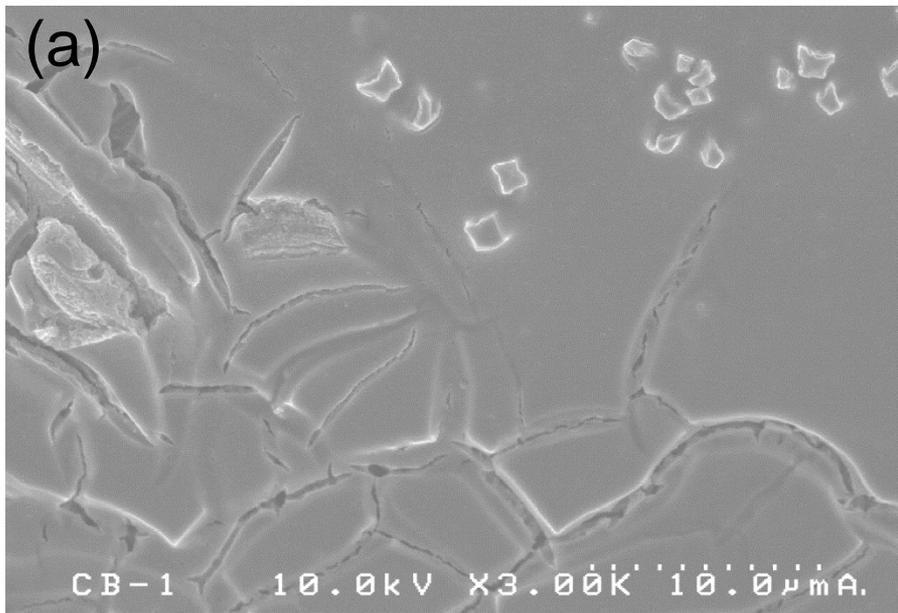(a); pristine, (b); used for 12 years.

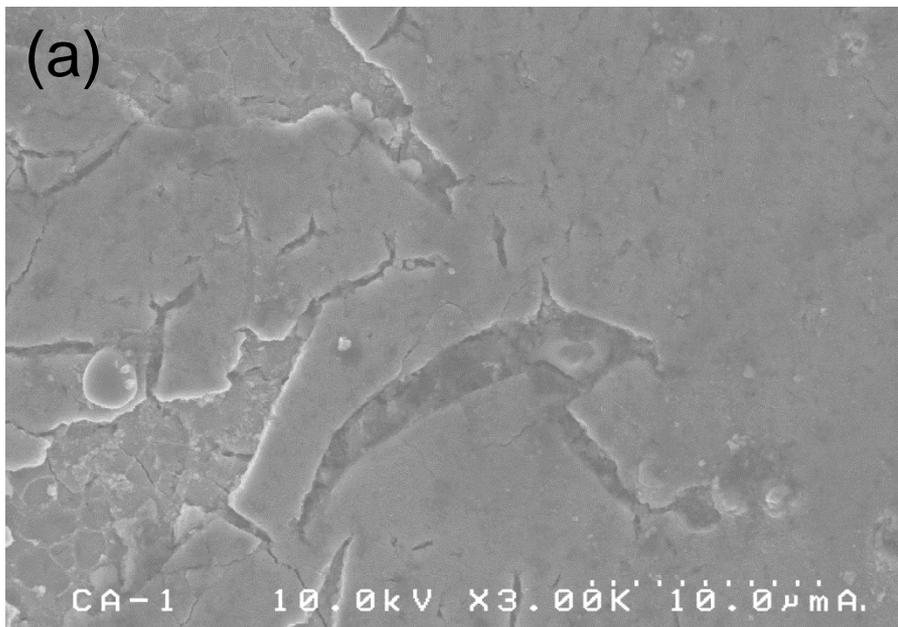Fig. 6   X-ray diffraction patterns of the pristine and the used RuO_2-TiO_2/Ti anodes.
(a); pristine, (b); used for 12 years.

Fig. 7   HR-SEM images at various magnifications of the pristine IrO_2-RuO_2-TiO_2/Ti anode.

Fig. 8   HR-SEM images at various magnifications of the IrO_2-RuO_2-TiO_2/Ti anode used for 15 years.

Fig. 9   Cross-section SEM images of the pristine and used IrO_2-RuO_2-TiO_2/Ti anodes
(a); pristine, (b); used for 15 years. The IrO_2-RuO_2-TiO_2/Ti anodes were coated with copper to stabilize the oxide layer towards the cross-sectional cutting.

Fig. 10   SEM images with the point analysis data determined by the HR-AES for the pristine and the used IrO_2-RuO_2-TiO_2/Ti anodes.
(a); pristine, (b); used for 15 years.

Fig. 11   X-ray diffraction patterns of for the pristine and the used IrO_2-RuO_2-TiO_2/Ti anodes.

(a)

(b)

Y.Takasu et al. Fig. 1

(a) CB-1   10.0kV X3.00K 10.0μmA.

(b) CB-1   15.0kV X10.0K 3.00μmA.

(c) CB-1   15.0kV X50.0K 600nmA.

(d) CB-1   15.0kV X200K   150nmA.

Y.Takasu et al. Fig. 2

(a) CA-1 10.0kV X3.00K 10.0μmA.

(b) CA-1 15.0kV X10.0K 3.00μmA.

(c) CA-1 15.0kV X50.0K 600nmA.

(d) CA-1 15.0kV X200K 150nmA.

Y.Takasu et al. Fig. 3

(a) G Cu Ti 5 μm

(b) Cu Ti 5 μm

Y.Takasu et al. Fig. 4

(a)

Ru,Ti,O   Ti,O   Ru,Ti,O   Ti,O

10/19/01 10.0kV 10.0kX   1.0μm
Sample CB

(b)

Ti,O   Ti,O   Ti,O   Ti,O

10/19/01 10.0kV 10.0kX   1.0μm
Sample CA

Y.Takasu et al. Fig. 5

R(200)+Ti

100 cps

R(101)
+ Ti

R(110)

Ti

R(211)

Ti

(b)

(a)

Intensity / cps

20   40   60   80

2θ / degree (CuKα)

Y.Takasu et al. Fig. 6

(a) BB-1 10.0kV X3.00K 10.0μmA.

(b) BB-1 15.0kV X10.0K 3.00μmA.

(c) BB-1 15.0kV X50.0K 600nmA.

(d) BB-1 15.0kV X200K 150nmA.

Y.Takasu et al. Fig. 7

(a) BA-1   10.0kV X3.00K 10.0μmA.

(b) BA-1   15.0kV X10.0K 3.00μmA.

(c) BA-1   15.0kV X50.0K 600nmA.

(d) BA-1   15.0kV X200K 150nmA.

Y.Takasu et al. Fig. 8

(a)

Cu

Ti

5 μm

(b)

Cu

Ti

5 μm

Y.Takasu et al. Fig. 9

(a) Ru,Ir,Ti,O Ti,O Ru,Ir,Ti,O Ir,Ti,O

(b) Ru,Ir,O Ru,Ir,O Ru,Ir,O Ti,O
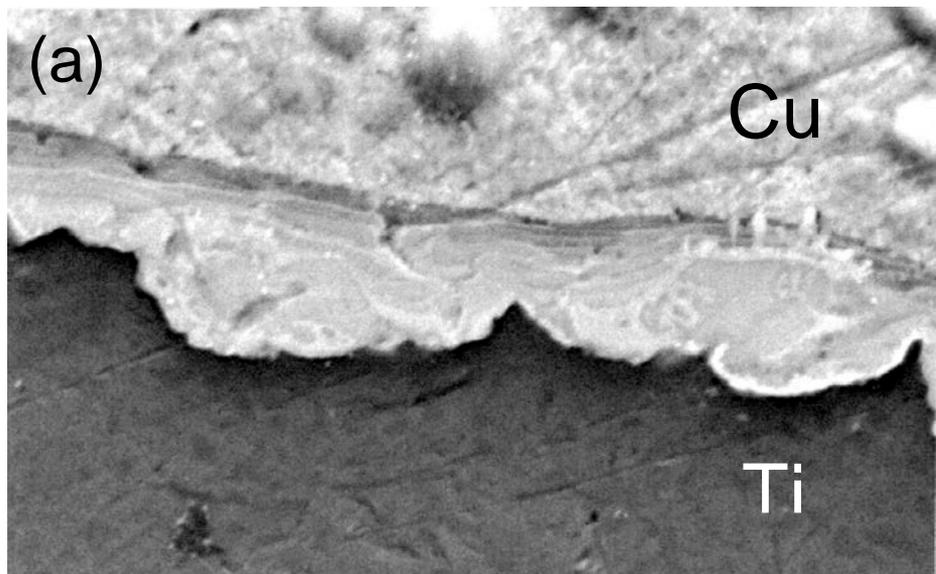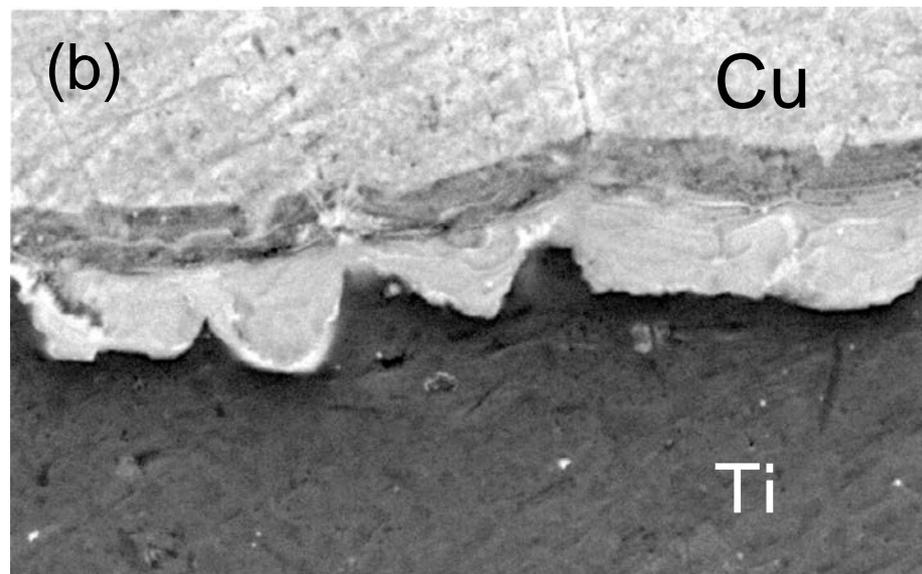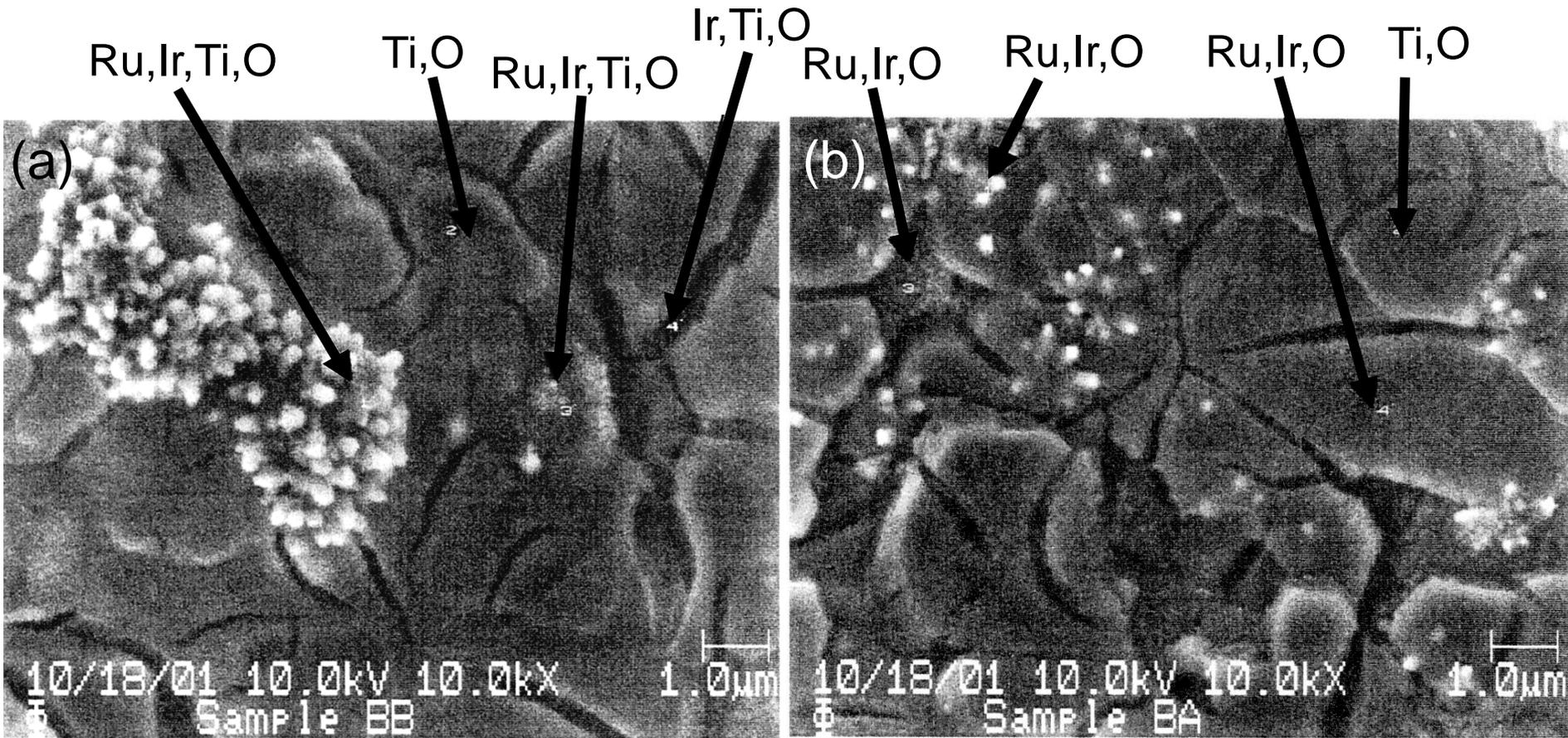
10/18/01 10.0kV 10.0kX 1.0μm Sample BB

10/18/01 10.0kV 10.0kX 1.0μm Sample BA

Y.Takasu et al. Fig. 10

Y.Takasu et al. Fig. 11